Phosphorus adsorption on iron-coated sand under reducing conditions

Victoria Barcala[1,2], Stefan Jansen[3], Jan Gerritse[3], Stefan Mangold[4], Andreas Voegelin[5], and Thilo Behrends[2]

[1] Inland Water Systems, Deltares, Daltonlaan 600, 3584 BK Utrecht, The Netherlands

[2] Department of Earth Sciences, Faculty of Geosciences, Utrecht University, 8 Princetonlaan, 3584 CB Utrecht, The Netherlands

[3] Deltares, Unit Subsurface and Groundwater Systems, Daltonlaan 600, 3584 BK, Utrecht, The Netherlands

[4] Karlsruhe Institute of Technology, Institute for Photon Science and Synchrotron Radiation, D-76344 Eggenstein-Leopoldshafen, Germany

[5] Eawag, Swiss Federal Institute of Aquatic Science and Technology, Ueberlandstrasse 133, CH-8600 Duebendorf, Switzerland

Correspondence: victoria.barcalapaolillo@deltares.nl

The supplementary material includes: video of ICS drain construction, XAS spectra, images of the treatment bottles during the microcosm-experiment, SEM-EDX results, chemical equations used for stociochemical calculations, mass balance of Fe losses in the field, and tables with water quality results.

Video link

https://www.youtube.com/watch?v=5ycj5CCzfpw

XAS results

The X-ray absorption near-edge structure (XANES) and the extended X-ray absorption fine structure (EXAFS) spectra of samples and references are shown in figure S1. The inspection of the sample spectra indicated that three reference spectra were required to describe the sample spectra by LCF: (i) silicate-containing ferrihydrite (Fh-Si) formed by the oxidation of Fe(II) in bicarbonate-buffered silicate-containing synthetic groundwater, (ii) 2-line ferrihydrite (2L-Fh) synthesized by the forced hydrolysis of a concentrated ferric iron solution (Schwertmann and Cornell, 1991) (both spectra from (Senn et al., 2017)), and (iii) mackinawite (FeS; spectrum kindly provided by Mingkai Ma, Utrecht University). Silicate-containing ferrihydrite exhibits a similar degree of edge-sharing linkage of Fe(III)-octahedra but a lower degree of corner-sharing linkage than 2-line ferrihydrite, due to the inhibiting effect of Si on corner-sharing Fe(III)-octahedra linkage. The two ferrihydrite references thus served to describe ferrihydrite with a level of Fe(III)-polymerization slightly varying from the reference materials. Indeed, the spectrum of the fresh unreacted Fe-coated sand closely matched the reference spectrum of silicate-containing ferrihydrite obtained by Fe (II) oxidation in bicarbonate-buffered solution in the presence of silicate (Senn et al., 2015), whereas LCF analysis of both the XANES and EXAFS spectra (Table S1) returned a minor contribution for the 2-line ferrihydrite (2L-Fh). This result was in good agreement with XAS characterization results for Fe in Fe-sludge and ICS derived from drinking water treatment (Chardon et al. 2021; Koopmans et al. 2020)and indicated that Fe in the coatings was contained in ferrihydrite with a slightly higher degree of polymerization than the silicate-containing ferrihydrite (Fh-Si) reference, possibly because of the aging of the coatings over the duration of sand used in water treatment.

Three of the reacted sand samples closely matched the unreacted fresh sand. Nevertheless, minor but systematic differences were observed relative to the fresh sand, most notably a slight increase of the spectral feature at 7.5 $Å^{-1}$ (see overlay of spectrum of fresh sand in figure S1).

These small differences may point to a slight increase in ferrihydrite polymerization during incubation, but for sure indicated that no substantial formation of a more crystalline Fe(III)-(hydr)oxide had occurred. The spectrum of the reacted sample 4 more distinctly differed from the fresh ICS. LCF analysis of the respective XANES and EXAFS spectra indicated that this difference could be described by a contribution of 7% (XANES) to 13% (EXAFS) FeS.

Because of the apparent signs of Fe sulfidization in the non-sterile incubation experiment with added C source (acetate; anoxic), and because the sample label of the reacted sample 4 did not match with this treatment, we noted that the reacted samples must have been misplaced during pellet preparation or sample mounting in the glove box. Nevertheless, it is highly plausible that the spectrum of the reacted sample 4 corresponded to the experiment in which Fe sulfidation was inferred from color changes, solution chemistry and microscopy. We therefore conclude from the XAS results that in the non-sterile experiment with added acetate, about 10% of the Fe was transformed into FeS during incubation, whereas in the sterile control and the experiment without acetate addition, no such transformation occured.

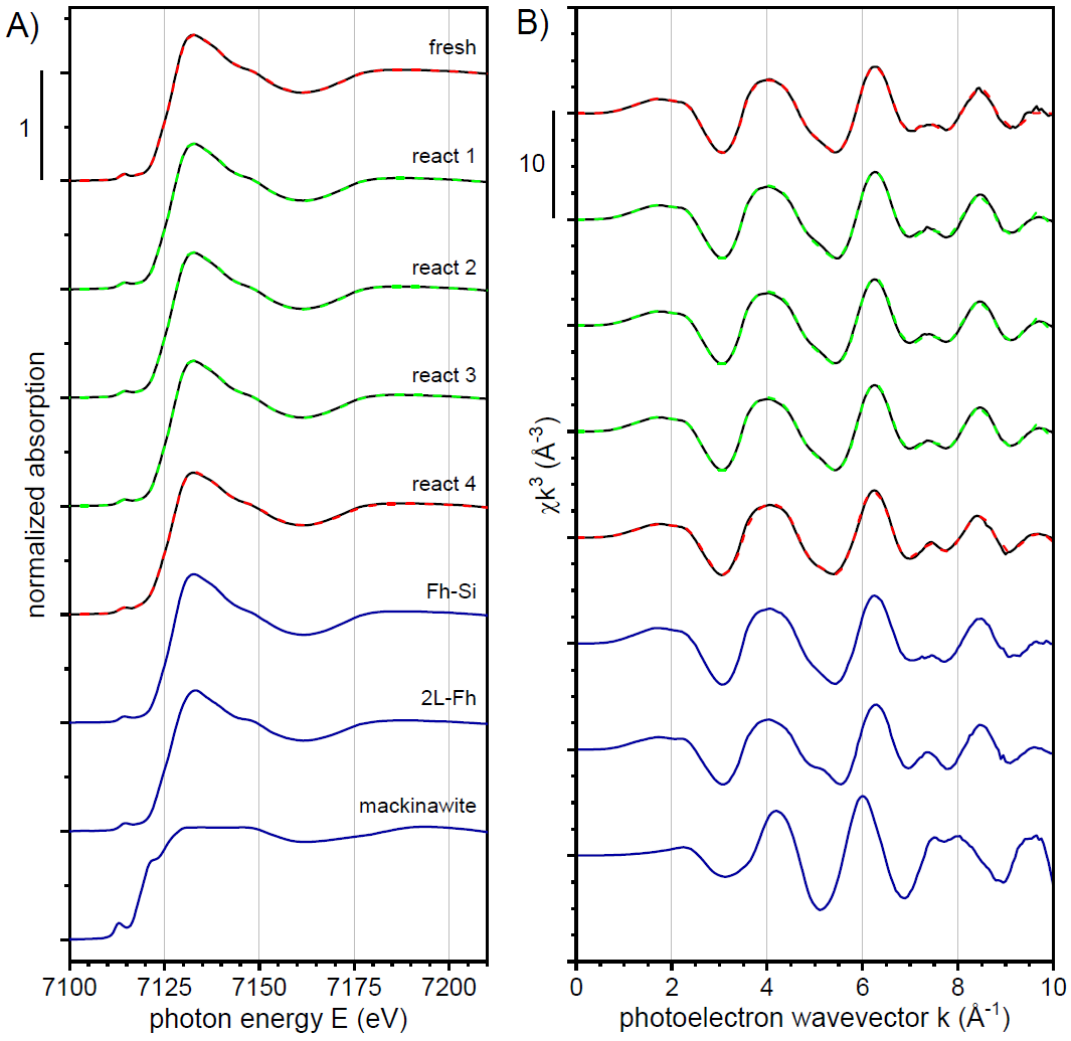

Figure S1. XANES and EXAFS spectra of the fresh unreacted Fe-coated sand and of four reacted samples in comparison to reference spectra of Fe(II)-derived silicate-containing ferrihydrite, of 2-line ferrihydrite and mackinawite (FeS). Red dashed spectra are linear reconstructions based on the LCF results listed in Table S1. Green dashed spectra represent the spectrum of the fresh unreacted sand.

Table S1. Linear combination fit results for the spectra of fresh unreacted sand and for the reacted sample 4.

		Fh-Si	2L-Fh	FeS	sum	r-factor
fresh sand	XANES	0.75	0.25	-	1.00	0.0001
	EXAFS	0.85	0.13	-	0.99	0.0024
reacted sample 4	XANES	0.58	0.34	0.07	1.00	0.0001
	EXAFS	0.61	0.26	0.13	1.00	0.0065

Pictures from microcosm experiment

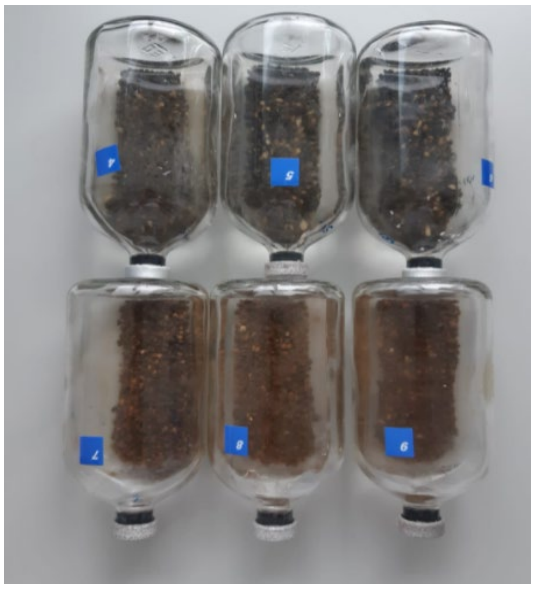

Figure S2. Observable changes in incubation: ICS grains in anoxic treatment with acetate addition turned black (top). Bottles without acetate addition (bottom) used as reference.

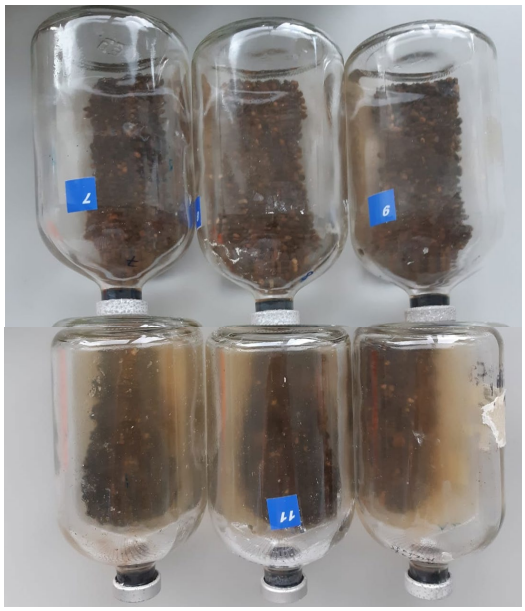

Figure S3. Observable changes in incubation: bottles with Moderately reducing addition were less transparent and had whitish precipitates (bottom). Bottles without acetate addition (top) used as reference

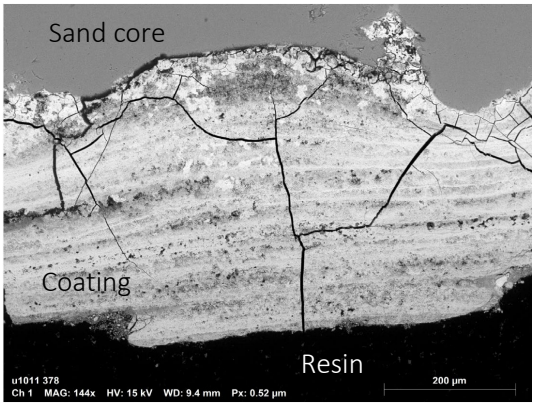

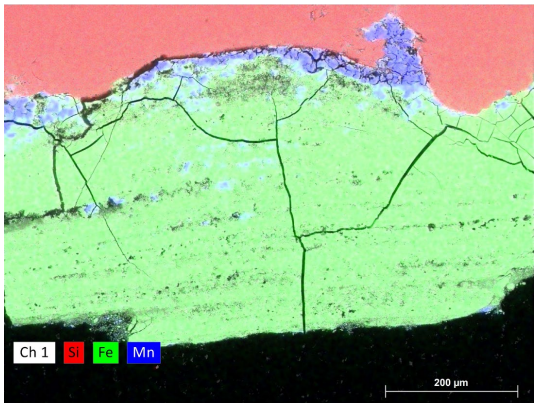

Atomic concentration [%]

Spectrum	Carbon	Oxygen	Silicon	Calcium	Iron
V1 1	0.00	64.70	35.30		
V1 2	0.00	64.46	35.54		
V1 3	0.00	69.19	6.50	2.30	22.02
Mean	**0.00**	**66.11**	**25.78**	**2.30**	**22.02**
Sigma	**0.00**	**2.66**	**16.70**	**0.00**	**0.00**
SigmaMean	**0.00**	**1.54**	**9.64**	**0.00**	**0.00**

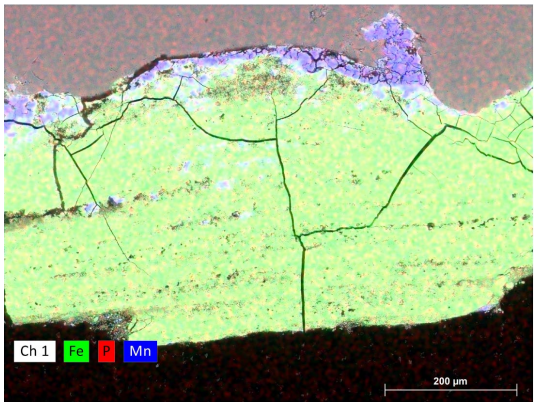

Figure S4. SEM image of ICS grain cross-section before treatment (left), EDX elemental map (right). The sand core is rich in silica, the coating is made of iron (hydr)oxides with manganese (hydr)oxides in separated areas. Points V1 and V2 were taken in the sand core and point V3 on the coating.

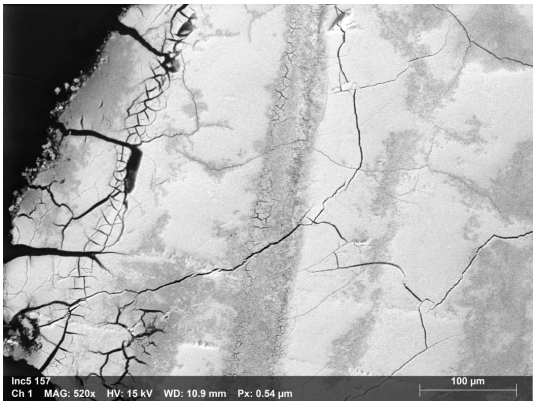

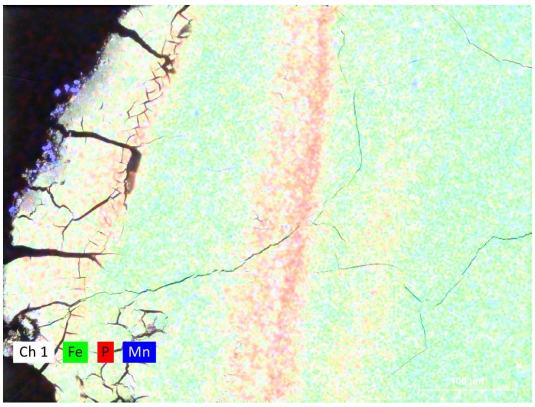

Element	At. No.	Netto	Mass [%]	Mass Norm. [%]	Atom [%]	abs. error [%] (1 sigma)	rel. error [%] (1 sigma)
Oxygen	8	236067	28.14	37.87	66.44	3.08	10.94
Iron	26	169628	41.53	55.88	28.09	1.24	2.99
Silicon	14	43802	2.59	3.49	3.49	0.13	5.16
Calcium	20	13757	1.35	1.81	1.27	0.07	5.00
Phosphorus	15	5940	0.35	0.47	0.42	0.04	11.38
Manganese	25	1621	0.30	0.41	0.21	0.04	12.31
Sodium	11	290	0.04	0.05	0.06	0.00	10.38
Aluminium	13	160	0.01	0.01	0.02	0.00	10.78
		Sum	**74.31**	**100.00**	**100.00**		

Figure S5. SEM image of ICS grain coating after adsorption and anoxic treatment with acetate addition (top-left), EDX elemental map of P(top-right), EDX analysis on a point in the high P red zone (bottom). Molar P/Fe ratio of 0.015 is in the range of typical ratios in fresh ICS

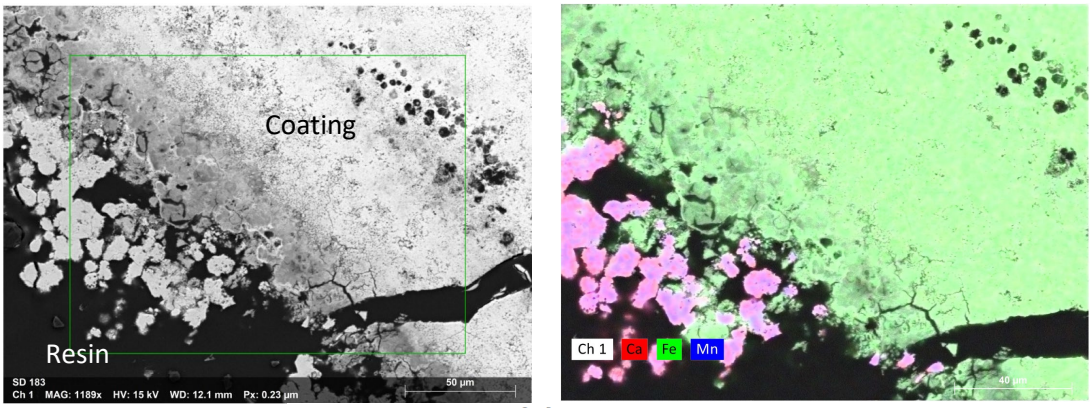

Atomic concentration [%]

Spectrum	Carbon	Oxygen	Calcium	Manganese
SD 761	22.69	61.59	14.32	1.39
SD 762	18.67	67.21	11.82	2.30
SD 763	18.51	66.56	12.62	2.30
SD 764	19.77	65.51	12.74	1.99
Mean	**19.91**	**65.22**	**12.88**	**2.00**
Sigma	**1.94**	**2.52**	**1.05**	**0.43**
SigmaMean	**0.97**	**1.26**	**0.52**	**0.21**

Figure S6. SEM image of ICS grain coating in treatment with Moderately reducing addition (top-left), EDX elemental map of Mn and Ca (top-right), EDX analysis on 4 different points from the Ca-Mn particles (bottom)

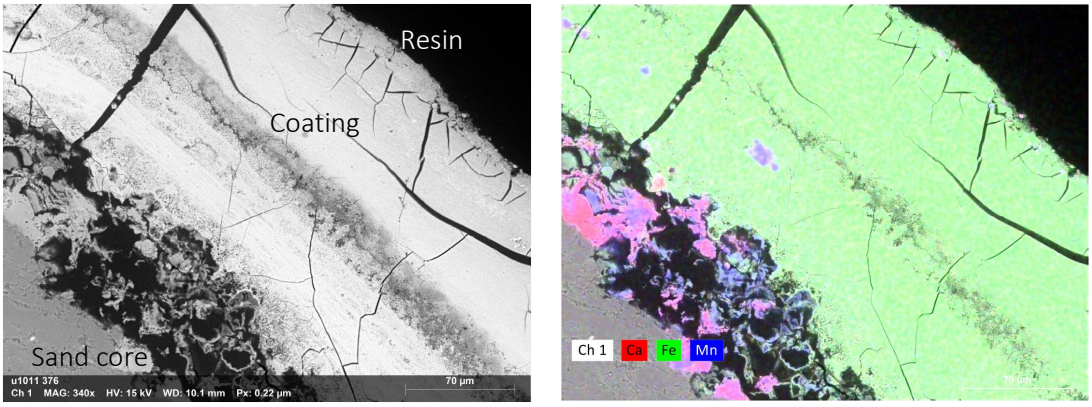

Figure S7. SEM image of ICS grain coating in treatment with Moderately reducing addition (left), EDX elemental map of Fe, Mn and, Ca(right), The Ca-Mn particles formed not only on the outside of the grain but on macropores or inner areas with originally high Mn.

Grain size distribution of the ICS

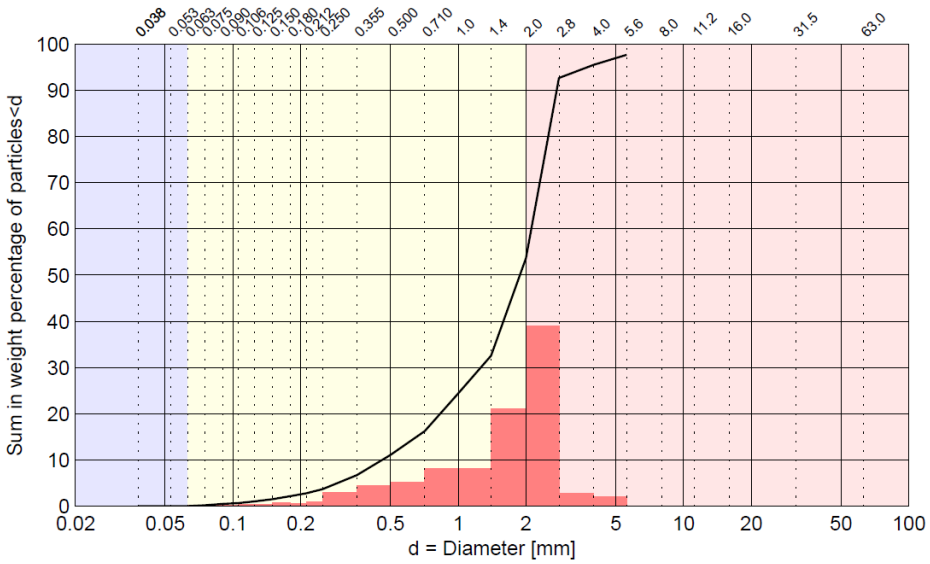

Symbol	Value
d_{10} [mm]	0.460
d_{15} [mm]	0.653
d_{50} [mm]	1.880
d_{60} [mm]	2.113
d_{60}/d_{10} [–]	4.6
d_{90}/d_{10} [–]	6.0

Chemical equations used for stoichiometrically calculations

Equations 1 and 2 represent the dissolution of Fe and Mn, mediated by microorganisms as *Geobacter* that use acetate as a carbon source and Fe and Mn (hydr)oxides as electron acceptors (Islam et al. 2004; Villinski, Saiers, and Conklin 2003). Equations 3 and 4 represent Fe (II) re-oxidation by Mn (IV) (Postma and Appelo 2000). Equation 5 represents the precipitation of manganese containing calcium carbonates. Equations 6 and 7 represent FeS precipitation as microbes reduced sulfate from the coating and groundwater (Van Beek et al. 2021; Finke, Vandieken, and Jorgensen 2007; Kwon et al. 2016; Zhang et al. 2021). Equation 8, 9, and 10 represents the possible Feammox reactions (Zhu et al. 2022) and equation 11 denitrification.

$$4\,Mn^{4+} + CH_3COO^- + 4H_2O \rightarrow Mn^{2+} + 2HCO_3^- + 9H^+ \quad (1)$$

$$8\,Fe^{3+} + CH_3COO^- + 4\,H_2O \rightarrow 8\,Fe^{2+} + 2HCO_3^- + 9H^+ \quad (2)$$

$$2Fe^{2+} + MnO_2 + H_2O \rightleftarrows 2FeOOH + Mn^{2+} + 2H^+ \quad (3)$$

$$Fe^{2+} + MnOOH + H_2O \rightleftarrows FeOOH + Mn^{2+} \quad (4)$$

$$7Ca^{2+} + 8HCO_3^- + Mn^{2+} \rightarrow Ca_7Mn(CO_3)_{8\,(s)} + 8H^+ \quad (5)$$

$$CH_3COO^- + SO_4^{2-} \rightarrow 2HCO_3^- + HS^- \quad (6)$$

$$SO_4^{2-} + Fe^{2+} + 8e^- + 8H^+ \rightarrow FeS_{(s)} + 4\,H_2O \quad (7)$$

$$3Fe_2O_3 + 2NH_4 + 10H^+ \rightarrow 9H_2O + 6Fe^{2+} + N_2 \quad (8)$$

$$3Fe_2O_3 + NH_4 + 10H^+ \rightarrow 7H_2O + 6Fe^{2+} + NO_2^- \quad (9)$$

$$4Fe_2O_3 + NH_4 + 14H^+ \rightarrow 9H_2O + 8Fe^{2+} + NO_3^- \quad (10)$$

$$\mathbf{2NO_3^- + 10e^- + 12H^+ \rightarrow N_2 + 6H_2O} \quad \mathbf{(11)}$$

Mass balance of Iron losses in the field per linear meter of ICS enveloped drain

Mass of Iron: each linear meter of drain, has approximately 0.015 m^3 of ICS, with a density of 1770 kg/m^3, and an iron content of 0.127 gFe/gICS, we get there are 26.5 kg-Fe/m or 474 mol-Fe/m.

Water balance: drains are 10 m apart from each other, therefore each linear meter drains 10 m^2, the estimated early rainfall is 860 mm, the yearly evapotranspiration is 450 mm, and the seepage 36.5 mm. Assuming 70 % of the groundwater is transported through the drains and the flow direction is vertical through the ICS layer, we get 3125.5 L/m/year.

Available carbon load: the measured DOC in the groundwater is 19.5 mg/L, not all the carbon will react in the drains, some may be recalcitrant organic matter, and some may not have enough time to react. If 100 % of DOC is consumed 61 g-C/m/year are available and if 10 % is consumed 6 g-C/m/year.

Balance: When 12 g (1 mol) of C are oxidized going from C(0) to C(IV) oxidation state, 4 electrons are transferred to reduce 4 mol Fe (III) to Fe (II). Therefore, if 100 % DOC is oxidized 20 mol-Fe/m/year are reduced, and if 10 % DOC is oxidized 2 mol-Fe/m/year are reduced. If we express it as a percentage of the original mass of iron per meter of drain, we get: 4 % and 0.4% could be reduced per linear meter per year.

P removal: From the field measurements, it seems reasonable to assume a P inflow concentration of 4.5 mg-P/L and outflow of 1.2 mg-P/L (73 % removal efficiency). If 3125.5

131 L/m/year are drained and the removal efficiency does not decrease with time, 10.31 g-P/m/year
132 (0.3 mol/m/year) would be removed.

133 Filter lifespan: It is possible now to estimate when (n_{year}) a 0.10 P/Fe molar ratio would be
134 reached if 100 % or 10 % of the DOC is used for iron reduction and the initial P/Fe_0 is 0.013.

135 $$P/Fe_{n_{year}=} P/Fe_0 + \frac{n_{year} \cdot 0.3 molP/year/m}{474 molFe/year/m - \%_{DOC} \cdot n_{year} \cdot 20 molFe/year/m} < 0.10$$

136 If 100 % DOC is used in iron reduction a 0.10 P/Fe molar ratio is reached after 20 years and if
137 10 % DOC is used a 0.10 P/Fe molar ratio is reached after 80 years.

138 **Water quality results**

139 **Table S2.** Average of triplicate bottles in different treatments in the microcosm experiment

Microcosm	Day	P (mg-P/L)	Fe II (mg/L)	Tot Fe (mg/L)	Mn (mg/L)	Acetate (mg/L)	Ca (mg/L)	SO4 (mg-S/L)
Autoclaved control	1	8.31	0.94	1.70	0.92	0	65.24	3.4
Strongly reducing	1	8.32	0.96	1.72	0.89	0	65.24	3.4
Weakly reducing	1	8.32	0.91	1.68	0.95	0	65.24	3.4
Moderately reducing	1	8.31	0.95	1.57	0.98	0	65.24	3.4
Autoclaved control	2	0.02	0.00	0.00	0.92	24		
Autoclaved control	2	0.02	0.00	0.00	9.58	24		
Strongly reducing	2	0.06	0.00	0.00	0.15	2		
Weakly reducing	2	0.05	0.00	0.00	0.09	1		
Moderately reducing	2	0.17	0.01	0.03	0.02	2		
Autoclaved control	8	0.01	0.13	0.10	8.92	0		
Strongly reducing	8	0.01	0.00	0.00	1.60	0		
Weakly reducing	8	0.02	0.03	0.05	1.58	0		
Moderately reducing	8	0.02	0.00	0.00	0.00	0		
Autoclaved control	10	0.01	0.03	0.00	10.25	2316		
Strongly reducing	10	0.00	0.02	0.13	1.40	2316		
Weakly reducing	10	0.01	0.00	0.00	0.97	0		
Moderately reducing	10	0.00	0.00	0.00	0.00	2316		
Autoclaved control	13	0.01	0.02	0.02	9.35	507		
Strongly reducing	13	0.01	0.00	0.00	8.63	633		
Weakly reducing	13	0.01	0.00	0.00	2.92	11		
Moderately reducing	13	0.00	0.01	0.04	10.32	550		
Autoclaved control	15	0.02	0.04	0.05	10.90	491		
Strongly reducing	15	0.02	4.10	4.15	24.79	536		
Weakly reducing	15	0.01	0.00	0.04	2.22	0		
Moderately reducing	15	0.01	0.01	0.03	9.45	493		

Autoclaved control	17	0.01	0.03	0.05	10.46	467		
Strongly reducing	17	0.03	5.43	5.49	12.42	463		
Weakly reducing	17	0.01	0.01	0.03	1.96	0		
Moderately reducing	17	0.00	0.07	0.10	5.77	421		
Autoclaved control	17	0.02	0.03	0.05	11.50	447		
Strongly reducing	20	0.03	3.31	3.29	5.69	394		
Weakly reducing	20	0.01	0.01	0.02	1.38	0		
Moderately reducing	20	0.00	0.05	0.19	3.53	373		
Autoclaved control	20	0.01	0.03	0.00	10.79	436		
Strongly reducing	22	0.04	2.61	2.40	3.80	353		
Weakly reducing	22	0.01	0.01	0.01	1.73	0		
Moderately reducing	22	0.00	0.12	0.20	2.73	338		
Autoclaved control	22	0.01	0.03	0.00	10.79	436		
Strongly reducing	24	0.02	1.80	1.99	3.00	328		
Weakly reducing	24	0.01	0.03	0.09	1.85	0		
Moderately reducing	24	0.01	0.16	0.39	2.23	304		
Autoclaved control	24	0.01	0.04	0.01	10.15	407		
Strongly reducing	27	0.04	1.80	1.80	2.30	315		
Weakly reducing	27	0.01	0.01	0.01	1.83	0		
Moderately reducing	27	0.03	0.24	0.63	1.73	231		
Autoclaved control	27	0.01	0.03	0.03	9.86	383		
Strongly reducing	29	0.03	1.79	1.80	2.21	236		
Weakly reducing	29	0.01	0.00	0.00	1.90	1		
Moderately reducing	29	0.03	0.26	0.58	1.32	176		
Autoclaved control	31	0.11	0.01	0.06	9.52	401	340.1	9.9
Strongly reducing	31	0.18	1.44	1.45	1.43	264	18.4	7.8
Weakly reducing	31	0.07	0.16	0.03	1.82	0	144.2	10.4
Moderately reducing	31	0.11	0.46	0.54	0.90	155	11.3	8.9
Autoclaved control	36	0.02	0.03	0.05	9.97	367		
Strongly reducing	36	0.06	1.90	1.98	1.96	4		
Weakly reducing	36	0.01	0.59	0.89	1.87	0		
Moderately reducing	36	0.06	0.01	0.23	1.70	0		
Autoclaved control	38	0.01	0.01	0.05	9.09	335		
Strongly reducing	38	0.05	1.47	1.60	1.64	0		
Weakly reducing	38	0.01	0.05	0.06	1.94	0		
Moderately reducing	38	0.04	0.39	0.55	0.72	0		
Autoclaved control	41	0.01	0.03	0.06	8.65	0		
Strongly reducing	41	0.06	1.47	1.51	1.50	0		
Weakly reducing	41	0.00	0.01	0.04	1.78	0		
Moderately reducing	41	0.03	0.30	0.38	0.57	0		
Autoclaved control	43	0.01	0.00	0.13	7.93	0	231.3	9.7
Strongly reducing	43	0.06	1.48	1.52	0.86	0	8.50	7.3
Weakly reducing	43	0.00	0.04	0.08	1.71	0	103.1	9.9
Moderately reducing	43	0.03	0.38	0.59	0.56	0	7.73	8.8
Autoclaved control	45	0.01	0.00	0.13	7.93	0	236.0	9.6
Strongly reducing	45	0.05	1.40	1.40	0.02	0	8.56	7.2

Weakly reducing	45	0.00	0.04	0.04	1.37	0	115.0	10.3
Moderately reducing	45	0.03	0.52	0.64	0.10	0	8.02	9.0

Table S4. PH in microcosms. Day 1 was measured with electrode (877, Mtrohm Titrino) and days 31 and 45 controlled with pH paper (Merk).

PH	Day 1	Day 31	Day 45
Autoclaved control	6.66	6.5-7	6.5-7
Strongly reducing	6.67	7.0	7.0
Moderately reducing	6.68	6.5	6.0
Weakly reducing	6.80	8.0-8.5	8.0

Table S5. Profiles of A and B fields made with GVP. Samples filtered (0.45um)

Field	Depth	pH	ORP (mV)	Tot Fe (mg/L)	Mn (mg/L)	P (mg-P/L)	P/Fe (molar)	Cl /Br ratio	NO3 (mg-N/L)	SO4 (mg-S/L)	NH4 (mg-N/L)
A	-101	7.27	-135	0.1	1.0	11.4	174.0	447.4	0.02	25.9	5.8
A	-124	7.21	-160	0.1	1.5	10.4	157.9	312.7	0.02	18.5	5.4
A	-205	7.2	-150	4.3	2.8	11.2	4.7	191.6	0.02	0.03	12.3
A	-240	6.9	-125	0.4	2.3	10.9	49.7	166.2	0.36	0.03	12.9
A	-265	7	-127	1.2	1.9	12.1	18.9	167.0	0.02	0.03	13.6
A	-300	6.9	-175	8.2	4.2	9.6	2.1	156.8	0.02	0.03	16.1
B	-120	7.76	-55	2.9	1.6	2.5	1.6	367.7	0.0	6.10	1.1
B	-148	7.46	-100	3.7	1.7	2.5	1.2	343.4	0.0	11.3	1.5
B	-181	7.3	-120	4.9	1.6	1.7	0.6	315.0	0.02	12.5	1.2
B	-195	7.4	-75	5.1	2.1	1.7	0.6	312.7	0.0	12.1	1.2
B	-246	7.6	-120	5.5	1.7	1.8	0.6	313.6	0.07	12.3	1.1
B	-275	7.4	-110	5.4	3.0	2.1	0.7	315.6	0.07	12.2	1.0
B	-310	7.3	-120	4.8	1.8	1.8	0.7	311.9	0.02	11.7	1.1
B	-340	7.3	-100	4.8	2.3	1.7	0.6	303.4	0.02	9.9	1.3
B	-372	7.3	-100	4.6	2.0	1.2	0.5	298.2	0.02	9.6	1.4

References

Van Beek, C. G. E. M., D. G. Cirkel, M. J. de Jonge, and N. Hartog. 2021. "Concentration of Iron(II) in Fresh Groundwater Controlled by Siderite, Field Evidence." *Aquatic Geochemistry* 27(1):49–61.

Chardon, WJ, Jan E. Groenenberg, Jos P. M. Vink, Andreas Voegelin, and Gerwin F. Koopmans. 2021. "Use of Iron-Coated Sand for Removing Soluble Phosphorus from Drainage Water." *Science of The Total Environment* 815:152738.

Finke, N., V. Vandieken, and B. Jorgensen. 2007. "Acetate, Lactate, Propionate, and Isobutyrate as Electron Donors for Iron and Sulfate Reduction in Arctic Marine Sediments, Svalbard." *Federation of European Microbiological Societies* (59):10–22.

Islam, Farhana S., Andrew G. Gault, Christopher Boothman, David A. Polya, John M. Chamok, Debashis Chatterjee, and Jonathan R. Lloyd. 2004. "Role of Metal-Reducing Bacteria in Arsenic Release from Bengal Delta Sediments." *Nature* 430(6995):68–71.

Koopmans, G. F., T. Hiemstra, C. Vaseur, W. J. Chardon, A. Voegelin, and J. E. Groenenberg. 2020. "Use of Iron Oxide Nanoparticles for Immobilizing Phosphorus In-Situ: Increase in Soil Reactive Surface Area and Effect on Soluble Phosphorus." *Science of the Total Environment* 711:135220.

Kwon, Man Jae, Edward J. O'Loughlin, Maxim I. Boyanov, Jennifer M. Brulc, Eric R. Johnston, Kenneth M. Kemner, and Dionysios A. Antonopoulos. 2016. "Impact of Organic Carbon Electron

Donors on Microbial Community Development under Iron-and Sulfate-Reducing Conditions." *PLoS ONE* 11(1).

Postma, D., and C. A. J. Appelo. 2000. "Reduction of Mn-Oxides by Ferrous Iron in a Flow System: Column Experiment and Reactive Transport Modeling." *Geochimica et Cosmochimica Acta* 64(7):1237–47.

Senn, Anna Caterina, Ralf Kaegi, Stephan J. Hug, Janet G. Hering, Stefan Mangold, and Andreas Voegelin. 2015. "Composition and Structure of Fe(III)-Precipitates Formed by Fe(II) Oxidation in Water at near-Neutral PH: Interdependent Effects of Phosphate, Silicate and Ca." *Geochimica et Cosmochimica Acta* 162:220–46.

Villinski, J., J. Saiers, and M. Conklin. 2003. "The Effects of Reaction-Product Formation on the Reductive Dissolution of MnO 2 by Fe (II)." *Environ. Sci. Technol.* 37(24):5589–96.

Zhang, Yuyang, Ziying Zhu, Yan Guang Liao, Zhi Dang, and Chuling Guo. 2021. "Effects of Fe(II) Source on the Formation and Reduction Rate of Biosynthetic Mackinawite: Biosynthesis Process and Removal of Cr(VI)." *Chemical Engineering Journal* 421(P1):129723.

Zhu, Ting-ting, Wen-xia Lai, Yao-bin Zhang, and Yi-wen Liu. 2022. "Science of the Total Environment Feammox Process Driven Anaerobic Ammonium Removal of Wastewater Treatment under Supplementing Fe (III) Compounds." *Science of the Total Environment* 804:149965.